

Fast Layout-Oblivious Tensor-Matrix Multiplication with BLAS

Cem Savaş Başsoy

Hamburg University of Technology, Schwarzenbergstrasse 95, Germany,
cem.bassoy@gmail.com

Abstract. The tensor-matrix multiplication is a basic tensor operation required by various tensor methods such as the ALS and the HOSVD. This paper presents flexible high-performance algorithms that compute the tensor-matrix product according to the Loops-over-GEMM (LoG) approach. Our algorithms can process dense tensors with any linear tensor layout, arbitrary tensor order and dimensions all of which can be runtime variable. We discuss different tensor slicing methods with parallelization strategies and propose six algorithm versions that call BLAS with subtensors or tensor slices. Their performance is quantified on a set of tensors with various shapes and tensor orders. Our best performing version attains a median performance of 1.37 double precision Tflops on an Intel Xeon Gold 6248R processor using Intel’s MKL. We show that the tensor layout does not affect the performance significantly. Our fastest implementation is on average at least 14.05% and up to 3.79 x faster than other state-of-the-art approaches and actively developed libraries like Libtorch and Eigen.

1 Introduction

Tensor computations are found in many scientific fields such as computational neuroscience, pattern recognition, signal processing and data mining [5, 12]. These computations use basic tensor operations as building blocks for decomposing and analyzing multidimensional data which are represented by tensors [6, 7]. Tensor contractions are an important subset of basic operations that need to be fast for efficiently solving tensor methods.

There are three main approaches for implementing tensor contractions. The Transpose-Transpose-GEMM-Transpose (TTGT) approach reorganizes (flattens) tensors in order to perform a tensor contraction using optimized General Matrix Multiplication (GEMM) implementations [1, 14]. Implementations of the GEMM-like Tensor-Tensor multiplication (GETT) method have macro-kernels that are similar to the ones used in fast GEMM implementations [10, 15]. The third method is the Loops-over-GEMM (LoG) approach in which BLAS are utilized with multiple tensor slices or subtensors if possible [2, 8, 11, 13]. Implementations of the LoG and TTGT approaches are in general easier to maintain and faster to port than GETT implementations which might need to adapt vector instructions or blocking parameters according to a processor’s microarchitecture.

In this work, we present high-performance algorithms for the tensor-matrix multiplication which is used in many numerical methods such as the alternating least squares method [6, 7]. It is a compute-bound tensor operation and has the same arithmetic intensity as a matrix-matrix multiplication which can almost reach the practical peak performance of a computing machine.

To our best knowledge, we are the first to combine the LoG approach described in [2] with the findings on tensor slicing for the tensor-matrix multiplication in [8]. Our proposed algorithms support dense tensors with any order, dimensions and any linear tensor layout including the first- and the last-order storage formats for any contraction mode all of which can be runtime variable. They compute the tensor-matrix product in parallel using efficient GEMM or batched GEMM without transposing or flattening tensors. Despite their high performance, all algorithms are layout-oblivious and provide a sustained performance independent of the tensor layout without tuning.

Moreover, every proposed algorithm can be implemented with less than 150 lines of C++ code where the algorithmic complexity is reduced by the BLAS implementation and the corresponding selection of subtensors or tensor slices. We have provided an open and free reference C++ implementation of all algorithms and a python interface for convenience. While we have used Intel’s MKL for our benchmarks, the user is free to choose any other library that provides the BLAS interface.

The following analysis quantifies the impact of the tensor layout, the tensor slicing method and parallel execution of slice-matrix multiplications with varying contraction modes. The runtime measurements of our implementations are compared with state-of-the-art approaches discussed in [10, 15] and actively developed libraries including Libtorch and Eigen. In summary, the main findings of our work are:

- A tensor-matrix multiplication can be implemented by an in-place algorithm with 1 `gemv` and 7 `gemm` calls, supporting all combinations of contraction mode, tensor order and dimensions for any linear tensor layout.
- Our fastest algorithm is on average 17% faster than Intel’s `gemm_batch` when the contraction and leading dimensions of the tensors are greater than 256.
- The proposed algorithms are layout-oblivious. Their performance does not vary significantly for different tensor layouts if the contraction conditions remain the same.
- Our fastest algorithm computes the tensor-matrix multiplication on average, by at least 14.05% and up to a factor of 3.79 faster than other state-of-the-art library implementations, including LibTorch and Eigen.

The remainder of the paper is organized as follows. Section 2 presents related work. Section 3 introduces some notation on tensors and defines the tensor-matrix multiplication. Algorithm design and methods for slicing and parallel execution are discussed in Section 4. Section 5 describes the test setup. Benchmark results are presented in Section 6. Conclusions are drawn in Section 7.

2 Related Work

The authors of [15] present a tensor-contraction generator TCCG and the GETT approach for dense tensor contractions that is inspired from the design of a high-performance GEMM. Their unified code generator selects implementations from generated GETT, LoG and TTGT candidates. Their findings show that among 48 different contractions 15% of LoG-based implementations are the fastest.

The author presents in [10] a runtime flexible tensor contraction library that uses GETT approach as well. He describes block-scatter-matrix algorithm which uses a special layout for the tensor contraction. The proposed algorithm yields results that feature a similar runtime behavior to those presented in [15].

The work in [8] introduces InTensLi, a framework that generates in-place tensor-matrix multiplication according to the LOG approach. The authors discuss optimization and tuning techniques for slicing and parallelizing the operation. With optimized tuning parameters, they report a speedup of up to 4x over the TTGT-based MATLAB tensor toolbox library discussed in [1].

In [2], the author presents LoG-based algorithms that compute the tensor-vector product. They support dense tensors with linear tensor layouts, arbitrary dimensions and tensor order. The presented approach is to divide into eight cases calling GEMV and DOT. He reports average speedups of 6.1x and 4.0x compared to implementations that use the TTGT and GETT approach, respectively.

Our work is inspired by [8] and [2]. We use lemmas for tensor slicing in [8] and generalize them for tensors with any linear tensor layouts. We have adapted the eight cases in [2] for tensor-matrix multiplication and combined it with the slicing method.

3 Background

Notation An order- p tensor is a p -dimensional array [9] where tensor elements are contiguously stored in memory. We write a , \mathbf{a} , \mathbf{A} and $\underline{\mathbf{A}}$ in order to denote scalars, vectors, matrices and tensors. If not otherwise mentioned, we assume $\underline{\mathbf{A}}$ to have a tensor order that is greater than 2. The p -tuple \mathbf{n} with $\mathbf{n} = (n_1, n_2, \dots, n_p)$ will be referred to as a dimension tuple with $n_r > 1$. We will use round brackets $\underline{\mathbf{A}}(i_1, i_2, \dots, i_p)$ or $\underline{\mathbf{A}}(\mathbf{i})$ to denote a tensor element where $\mathbf{i} = (i_1, i_2, \dots, i_p)$ is a multi-index. A subtensor is denoted by $\underline{\mathbf{A}}'$ and references elements of a tensor $\underline{\mathbf{A}}$. They are specified with p index ranges and form a selection grid. In this work, the index range shall either address all indices of a given mode or a single element that are given by single indices i_r with $1 \leq r \leq p$. Elements n'_r of a subtensor's dimension tuple \mathbf{n}' are therefore n_r if all indices of mode r are selected and 1 otherwise. We will annotate subtensors using only their non-unit modes such as $\underline{\mathbf{A}}'_{u,v,w}$ where $n_u > 1, n_v > 1$ and $n_w > 1$ and $1 \leq u \neq v \neq w \leq p$. It is sufficient to only provide non-unit modes as the remaining single indices correspond to the loop induction variables of the following algorithms. A subtensor is called a slice $\underline{\mathbf{A}}'_{u,v}$ if the full range selection of $\underline{\mathbf{A}}$ occurs with only two modes. A fiber $\underline{\mathbf{A}}'_u$ is a tensor slice with only one dimension greater than 1.

Linear Tensor Layouts We use a layout tuple $\boldsymbol{\pi} \in \mathbb{N}^p$ to encode all linear tensor layouts including the first-order or last-order layout. They contain permuted tensor modes whose priority is given by their index. For instance, the first- and last-order storage formats are given by $\boldsymbol{\pi}_F = (1, 2, \dots, p)$ and $\boldsymbol{\pi}_L = (p, p-1, \dots, 1)$. The general k -order tensor layout for an order- p tensor is given by the layout tuple $\boldsymbol{\pi}$ with $\pi_r = k - r + 1$ for $1 < r \leq k$ and r for $k < r \leq p$. An inverse layout tuple $\boldsymbol{\pi}^{-1}$ is defined by $\boldsymbol{\pi}^{-1}(\boldsymbol{\pi}(k)) = k$. Given a layout tuple $\boldsymbol{\pi}$ with p modes, the π_r -th element of a stride tuple is given by $w_{\pi_r} = \prod_{k=1}^{r-1} n_{\pi_k}$ for $1 < r \leq p$ and $w_{\pi_1} = 1$. Tensor elements of the π_1 -th mode are contiguously stored in memory. The location of tensor elements is determined by the tensor layout and the layout function. For a given tensor layout and stride tuple, a layout function $\lambda_{\mathbf{w}}$ maps a multi-index to a scalar index with $\lambda_{\mathbf{w}}(\mathbf{i}) = \sum_{r=1}^p w_r(i_r - 1)$. With $j = \lambda_{\mathbf{w}}(\mathbf{i})$ being the relative memory position of an element with a multi-index \mathbf{i} , reading from and writing to memory is accomplished with j and the first element's address of $\underline{\mathbf{A}}$.

Non-Modifying Flattening and Reshaping The flattening operation $\varphi_{r,q}$ transforms an order- p tensor $\underline{\mathbf{A}}$ to another order- p' view $\underline{\mathbf{B}}$ that has different a shape \mathbf{m} and layout $\boldsymbol{\tau}$ tuple of length p' with $p' = p - q + r$ and $1 \leq r < q \leq p$. It is related to the tensor unfolding operation as defined in [6, p.459] but neither changes the element ordering nor copies tensor elements. Given a layout tuple $\boldsymbol{\pi}$ of $\underline{\mathbf{A}}$, the flattening operation $\varphi_{r,q}$ is defined for contiguous modes $\hat{\boldsymbol{\pi}} = (\pi_r, \pi_{r+1}, \dots, \pi_q)$ of $\boldsymbol{\pi}$. Let $j = 0$ if $k \leq r$ and $j = q - r$ otherwise for $1 \leq k \leq p'$. Then the resulting layout tuple $\boldsymbol{\tau} = (\tau_1, \dots, \tau_{p'})$ of $\underline{\mathbf{B}}$ is given by $\tau_r = \min(\boldsymbol{\pi}_{r,q})$ and $\tau_k = \pi_{k+j} + s_k$ if $k \neq r$ where $s_k = |\{\pi_i \mid \pi_{k+j} > \pi_i \wedge \pi_i \neq \min(\hat{\boldsymbol{\pi}}) \wedge r \leq i \leq p\}|$. Elements of the corresponding shape tuple \mathbf{m} are given by $m_{\tau_r} = \prod_{k=r}^q n_{\pi_k}$ and $m_{\tau_k} = n_{\pi_{k+j}}$ if $k \neq r$.

The reshaping operation ρ transforms an order- p tensor $\underline{\mathbf{A}}$ to another order- p tensor $\underline{\mathbf{B}}$ with different shape \mathbf{m} and layout $\boldsymbol{\tau}$ tuples of length p . In this work, it permutes the shape and layout tuple simultaneously without changing the element ordering and without copying tensor elements. The operation ρ uses a permutation tuple $\boldsymbol{\rho} = (\rho_1, \dots, \rho_p)$ to only modify shape and layout tuples. Elements of the resulting shape tuple \mathbf{m} and the layout tuple $\boldsymbol{\tau}$ are given by $m_r = n_{\rho_r}$ and $\tau_r = \pi_{\rho_r}$, respectively.

Tensor-Matrix Multiplication (TTM) Let $\underline{\mathbf{A}}$ and $\underline{\mathbf{C}}$ be order- p tensors with shapes $\mathbf{n}_a = (n_1, \dots, n_q, \dots, n_p)$ and $\mathbf{n}_c = (n_1, \dots, n_{q-1}, m, n_{q+1}, \dots, n_p)$. Let \mathbf{B} be a matrix of shape $\mathbf{n}_b = (m, n_q)$. A mode- q TTM is denoted by $\underline{\mathbf{C}} = \underline{\mathbf{A}} \times_q \mathbf{B}$ where an element of $\underline{\mathbf{C}}$ is given by

$$\underline{\mathbf{C}}(i_1, \dots, i_{q-1}, j, i_{q+1}, \dots, i_p) = \sum_{i_q=1}^{n_q} \underline{\mathbf{A}}(i_1, \dots, i_q, \dots, i_p) \cdot \mathbf{B}(j, i_q) \quad (1)$$

with $1 \leq i_r \leq n_r$ and $1 \leq j \leq m$. Mode q is the *contraction mode* of the TTM with $1 \leq q \leq p$. The tensor-matrix multiplication generalizes the computational aspect of the two-dimensional case $\mathbf{C} = \mathbf{B} \cdot \mathbf{A}$ if $p = 2$ and $q = 1$. Its arithmetic

intensity is equal to that of a matrix-matrix multiplication and is not memory-bound. In the following, we assume that the tensors $\underline{\mathbf{A}}$ and $\underline{\mathbf{C}}$ have the same tensor layout $\boldsymbol{\pi}$. Elements of matrix $\underline{\mathbf{B}}$ can be stored either in the column-major or row-major format. Without loss of generality, we assume $\underline{\mathbf{B}}$ to have the row-major storage format in this work.

4 Algorithm Design

4.1 Sequential Algorithm

The sequential baseline algorithm for Eq. 1 can be implemented with a single C++ function that supports tensors with arbitrary order, dimensions and any linear tensor layout. It consists of nested recursion with a control flow that is akin to algorithm 1 in [3] consisting of two **if** statements with an **else** branch. The body of the first **if** statement contains a recursive call that skips the iteration over the dimension n_q when $r = \hat{q}$ with $\pi_r = q$ and $\hat{q} = \pi_q^{-1}$ where π^{-1} is the inverse layout tuple. The second **if** statement contains multiple recursive calls for the modes $1 \leq r \neq \hat{q} \leq p$ with different multi-indices. The **else** branch is the base case and consists of two loops that compute a fiber-matrix product. The outer loop iterates with j over the dimension m of $\underline{\mathbf{C}}$ and $\underline{\mathbf{B}}$. The inner loop iterates with i_q over the dimension n_q of $\underline{\mathbf{A}}$ and $\underline{\mathbf{B}}$ computing an inner product.

4.2 Baseline Algorithm with Contiguous Memory Access

The baseline algorithm accesses elements of $\underline{\mathbf{A}}$ and $\underline{\mathbf{C}}$ non-contiguously whenever $\pi_1 \neq q$. Matrix $\underline{\mathbf{B}}$ is contiguously accessed if i_q or j is incremented with unit-steps depending on the storage format of $\underline{\mathbf{B}}$. The access pattern can be improved by reordering tensor elements according to the storage format. However, copy operations reduce the overall throughput of the operation [13].

A better approach is to access tensor elements according to the tensor layout using the tensor layout tuple $\boldsymbol{\pi}$ as proposed in [3]. The modified algorithm 1 contiguously accesses memory for $\pi_1 \neq q$ and $p > 1$. Each recursion level adjusts only one multi-index element i_{π_r} with a stride w_{π_r} in line 5. With increasing recursion level and decreasing r , indices are incremented with smaller step sizes as $w_{\pi_r} \leq w_{\pi_{r+1}}$. The condition of the second **if** statement in line 4 is changed from $r \geq 1$ to $r > 1$. In this way, the mode- π_1 loop with index i_{π_1} and the minimum stride w_{π_1} are included in the base case which contains three loops performing a slice-matrix multiplication. The loop ordering are adjusted according to the tensor and matrix layout. The inner-most loop increments i_{π_1} and contiguously accesses tensor elements of $\underline{\mathbf{A}}$ and $\underline{\mathbf{C}}$. The second loop increments i_q with which elements of $\underline{\mathbf{B}}$ are contiguously accessed if $\underline{\mathbf{B}}$ is stored in the row-major format. The third loop increments j and could be placed as the second loop if $\underline{\mathbf{B}}$ is stored in the column-major format.

While spatial data locality is improved by adjusting the loop ordering, the temporal data locality of tensors $\underline{\mathbf{A}}$ and $\underline{\mathbf{C}}$ differ. Note that slice $\underline{\mathbf{A}}'_{\pi_1, q}$ is accessed

```

1 tensor_times_matrix(A, B, C, n, i, m, q, q̂, r)
2   if  $r = \hat{q}$  then
3     | tensor_times_matrix(A, B, C, n, i, m, q, q̂,  $r - 1$ )
4   else if  $r > 1$  then
5     | for  $i_{\pi_r} \leftarrow 1$  to  $n_{\pi_r}$  do
6       | | tensor_times_matrix(A, B, C, n, i, m, q, q̂,  $r - 1$ )
7   else
8     | for  $j \leftarrow 1$  to  $m$  do
9       | | for  $i_q \leftarrow 1$  to  $n_q$  do
10        | | | for  $i_{\pi_1} \leftarrow 1$  to  $n_{\pi_1}$  do
11          | | | | C( $i_1, \dots, i_{q-1}, j, i_{q+1}, \dots, i_p$ ) += A( $i_1, \dots, i_q, \dots, i_p$ ) · B( $j, i_q$ )

```

Algorithm 1: Modified baseline algorithm with contiguous memory access for the tensor-matrix multiplication. The tensor order must be greater than one and for the contraction mode $1 \leq q \leq p$ and $\pi_1 \neq q$ must hold. The algorithm needs to be initially called with $r = p$ where \mathbf{n} is the shape tuple of $\underline{\mathbf{A}}$ and m is the q -th dimension of $\underline{\mathbf{C}}$.

206 m times, fiber $\underline{\mathbf{C}}_{\pi_1}$ is accessed $\mathbf{n}(q)$ times and element $\underline{\mathbf{B}}(j, i_q)$ is accessed $\mathbf{n}(\pi_1)$
 207 times. While the specified fiber of $\underline{\mathbf{C}}$ can fit into first or second level cache, slice
 208 elements of $\underline{\mathbf{A}}$ are unlikely to fit in the local caches if the slice size $n_{\pi_1} \times n_q$
 209 is large leading to higher cache misses and suboptimal performance. Optimized
 210 tiling for better temporal data locality has been discussed in [4] which suggests
 211 to use existing high-performance BLAS implementations for the base case.

212 4.3 BLAS-based Algorithms with Tensor Slices

213 Algorithm 1 is the starting point for the BLAS-based algorithm which computes
 214 the tensor-matrix product with a `gemm` routine. Besides the illustrated algorithm,
 215 we have identified seven other cases where a single `gemm` call suffices to compute
 216 the tensor-matrix product even if the tensor order $p > 2$. In summary, there
 217 are eight cases with a single `gemm` call using different arguments which are listed
 218 in table 1. The list of `gemm` calls supports all linear tensor layout and has no
 219 limitation on tensor order and contraction mode. The arguments of `gemm` are
 220 chosen depending on the tensor order p , tensor layout π and contraction mode
 221 q except for the `CBLAS_ORDER` which is `CblasRowMajor`.

222 *Case 1* ($p = 1$): The tensor-vector product $\underline{\mathbf{A}} \times_1 \mathbf{B}$ can be computed with a
 223 `gemv` operation $\mathbf{a}^T \cdot \mathbf{B}$ where $\underline{\mathbf{A}}$ is an order-1 tensor, i.e. a vector \mathbf{a} of length n_1 .

224 *Case 2-5* ($p = 2$): If $\underline{\mathbf{A}}$ and $\underline{\mathbf{C}}$ are order-2 tensors, i.e. a matrix \mathbf{A} with
 225 dimensions n_1 and n_2 , then a single `gemm` suffices to compute the tensor-matrix
 226 product. If \mathbf{A} and \mathbf{C} have the column-major format with $\pi = (1, 2)$, `gemm` either
 227 executes $\mathbf{C} = \mathbf{A} \cdot \mathbf{B}^T$ for $q = 1$ or $\mathbf{C} = \mathbf{B} \cdot \mathbf{A}$ for $q = 2$. Note that `gemm` interprets
 228 \mathbf{C} and \mathbf{A} as matrices using the reshaping operation ρ with $\rho = (2, 1)$ in row-
 229 major format even though both are stored column-wise. If \mathbf{A} and \mathbf{C} have the

Case	Order p	Layout π	Mode q	Routine	T	M	N	K	A	LDA	B	LDB	LDC
1	1	-	1	gemv	-	m	n_1	-	B	n_1	<u>A</u>	-	-
2	2	(1, 2)	1	gemm	B	n_2	m	n_1	<u>A</u>	n_1	B	n_1	m
3	2	(1, 2)	2	gemm	-	m	n_1	n_2	B	n_2	<u>A</u>	n_1	n_1
4	2	(2, 1)	1	gemm	-	m	n_2	n_1	B	n_1	<u>A</u>	n_2	n_2
5	2	(2, 1)	2	gemm	B	n_1	m	n_2	<u>A</u>	n_2	B	n_2	m
6	> 2	any	π_1	gemm	B	\bar{n}_q	m	n_q	<u>A</u>	n_q	B	n_q	m
7	> 2	any	π_p	gemm	-	m	\bar{n}_q	n_q	B	n_q	<u>A</u>	\bar{n}_q	\bar{n}_q
8	> 2	any	π_2, \dots, π_{p-1}	gemm*	-	m	n_{π_1}	n_q	B	n_q	<u>A</u>	w_q	w_q

Table 1. Eight cases with **gemv** and **gemm** for the mode- q tensor-matrix multiplication. Arguments T, M, N, etc. of the BLAS are chosen with respect to the tensor order p , layout π and contraction mode q where T specifies if **B** is transposed. **gemm*** denotes multiple **gemm** calls with different tensor slices. Argument \bar{n}_q for case 6 and 7 is given by $\bar{n}_q = 1/n_q \prod_r n_r$. Matrix **B** has the row-major format.

row-major format with $\pi = (2, 1)$, **gemm** either executes $\mathbf{C} = \mathbf{B} \cdot \mathbf{A}$ for $q = 1$ or $\mathbf{C} = \mathbf{A} \cdot \mathbf{B}^T$ for $q = 2$. Note that the transposition of **B** is necessary for the cases 2,5 and independent of the chosen storage format.

Case 6-7 ($p > 2$): If the order of **A** and **C** is greater than 2 and if the contraction mode q is equal to π_1 (case 6), a single **gemm** with the depicted parameters executes $\mathbf{C} = \mathbf{A} \cdot \mathbf{B}^T$ and computes a tensor-matrix product **C** = **A** \times_{π_1} **B** for any storage layout of **A** and **C**. Tensors **A** and **C** are flattened with $\varphi_{2,p}$ to row-major matrices **A** and **C**. Matrix **A** has $\bar{n}_{\pi_1} = \bar{n}/n_{\pi_1}$ rows and n_{π_1} columns while matrix **C** has the same number of rows and m columns. If $\pi_p = q$ (case 7), Tensors **A** and **C** are flattened with $\varphi_{1,p-1}$ to column-major matrices **A** and **C**. Matrix **A** has n_{π_p} rows and $\bar{n}_{\pi_p} = \bar{n}/n_{\pi_p}$ columns while matrix **C** has m rows and the same number of columns. A single **gemm** executes $\mathbf{C} = \mathbf{B} \cdot \mathbf{A}$ and computes the tensor-matrix product **C** = **A** \times_{π_p} **B** for any storage layout of **A** and **C**. Note that in all cases no copy operation is performed in order to compute the desired contraction, see subsection 3.

Case 8 ($p > 2$): If the tensor order is greater than 2 with $\pi_1 \neq q$ and $\pi_p \neq q$, the modified baseline algorithm 1 is used to successively call $\bar{n}/(n_q \cdot n_{\pi_1})$ times **gemm** with different tensor slices of **C** and **A** in the base case. Each **gemm** computes one slice **C**' $_{\pi_1,q}$ of the tensor-matrix product **C** using the corresponding tensor slices **A**' $_{\pi_1,q}$ and the matrix **B**. The matrix-matrix product $\mathbf{C} = \mathbf{B} \cdot \mathbf{A}$ is performed by interpreting both tensor slices as row-major matrices **A** and **C** which have the dimensions (n_q, n_{π_1}) and (m, n_{π_1}) , respectively.

4.4 BLAS-Based Algorithms with Subtensors

Case 8 can be optimized by utilizing larger subtensors instead of tensor slices. This can be done by adding mergeable modes to the slice-matrix multiplication in which the subtensor can be flattened into a matrix without reordering ten-

256 sor elements. The flattening operation does not copy or reorder elements, see
 257 section 3 and lemma 4.1 in [8]. The number of mergeable modes is $\hat{q} - 1$ with
 258 $\hat{q} = \pi^{-1}(q)$ and the corresponding modes are $\pi_1, \pi_2, \dots, \pi_{\hat{q}-1}$. Applying flatten-
 259 ing $\varphi_{1,q-1}$ and reshaping ρ with $\rho = (2, 1)$ on a subtensor of $\underline{\mathbf{A}}$ with dimensions
 260 $n_{\pi_1}, \dots, n_{\pi_{\hat{q}-1}}, n_q$ yields a row-major matrix \mathbf{A} with shape $(n_q, \prod_{r=1}^{\hat{q}-1} n_{\pi_r})$. Anal-
 261 ogously, tensor $\underline{\mathbf{C}}$ becomes a row-major matrix with the shape $(m, \prod_{r=1}^{\hat{q}-1} n_{\pi_r})$.
 262 This description supports all linear tensor layouts and generalizes lemma 4.2
 263 in [8].

264 Algorithm 1 needs a minor modification so that `gemm` can be used with flat-
 265 tened subtensors instead of tensor slices. The modified algorithm therefor iter-
 266 ates only over modes larger than \hat{q} in the non-base case and hence omits the
 267 first \hat{q} modes $\pi_{1,\hat{q}} = (\pi_1, \dots, \pi_{\hat{q}})$ with $\pi_{\hat{q}} = q$. The conditions in line 2 and 4 are
 268 changed to $1 < r \leq \hat{q}$ and $\hat{q} < r$, respectively. The single indices of the subtensors
 269 $\underline{\mathbf{A}}'_{\pi_{1,\hat{q}}}$ and $\underline{\mathbf{C}}'_{\pi_{1,\hat{q}}}$ are given by the loop induction variables that belong to the
 270 π_r -th loop with $\hat{q} + 1 \leq r \leq p$.

271 4.5 Parallel BLAS-based Algorithms

272 The following paragraphs discuss three parallel approaches for the eighth case.
 273 Cases 1 to 7 already call a multi-threaded `gemm` and cannot be further optimized.

274
 275 **Sequential Loops and Multithreaded Matrix Multiplication** One straight
 276 forward approach is to use algorithm 1 as it is and to sequentially call a multi-
 277 threaded `gemm` in the base case of the algorithm as described in subsection 4.3.
 278 This is beneficial if $q = \pi_{p-1}$, the inner dimensions n_{π_1}, \dots, n_q are large or the
 279 outer-most dimension n_{π_p} is smaller than the available processor cores. How-
 280 ever, if the above conditions are not met, the processor cores might not be fully
 281 utilized where each multi-threaded `gemm` is executed with small subtensors. We
 282 will refer to this algorithm version as `<seq-loops,par-gemm>` that is executable
 283 with subtensors or tensor slices.

284 **Parallel Loops and Single or Multithreaded Matrix Multiplication** A
 285 more advanced version of the above algorithm executes a single-threaded `gemm`
 286 in parallel including all available (free) modes which depend on the slicing. If
 287 subtensors are used, all $\pi_{\hat{q}+1}, \dots, \pi_p$ modes are free. In case of tensor slices, only
 288 π_1 and $\pi_{\hat{q}}$ are free modes. The corresponding maximum degree of parallelism for
 289 both cases are $\prod_{r=\hat{q}+1}^p n_{\pi_r}$ and $\prod_{r=1}^p n_r / (n_{\pi_1} n_{\pi_{\hat{q}}})$, respectively.

290 Using tensor slices for the multiplication, $\underline{\mathbf{A}}$ and $\underline{\mathbf{C}}$ are flattened twice with
 291 $\varphi_{\pi_{\hat{q}+1}, \pi_p}$ and $\varphi_{\pi_2, \pi_{\hat{q}-1}}$. The resulting tensor is of order 4 with dimensions $n_{\pi_1},$
 292 $\hat{n}_{\pi_2}, n_q, \hat{n}_{\pi_4}$ where $\hat{n}_{\pi_2} = \prod_{r=2}^{\hat{q}-1} n_{\pi_r}$ and $\hat{n}_{\pi_4} = \prod_{r=\hat{q}+1}^p n_{\pi_r}$. In this way the tree-
 293 recursion has been transformed in two loops. The outer loop iterates over \hat{n}_{π_4}
 294 while the inner loop iterates over \hat{n}_{π_2} calling `gemm` with slices $\underline{\mathbf{A}}'_{\pi_{1,q}}$ and $\underline{\mathbf{C}}'_{\pi_{1,q}}$.
 295 Both loops are parallelized using `omp parallel for` together with the `collapse(2)`
 296 and the `num_threads` clause which specifies the thread number.

In case of the general subtensor-matrix approach, both tensors are flattened twice with $\varphi_{\pi_{\hat{q}+1}, \pi_p}$ and $\varphi_{\pi_1, \pi_{\hat{q}-1}}$. The resulting tensor is of order 3 with dimensions $\hat{n}_{\pi_1}, n_q, \hat{n}_{\pi_4}$ where $\hat{n}_{\pi_1} = \prod_{r=1}^{\hat{q}-1} n_{\pi_r}$ and $\hat{n}_{\pi_4} = \prod_{r=\hat{q}+1}^p n_{\pi_r}$. The corresponding algorithm consists of one loops which iterates over \hat{n}_{π_4} calling single-threaded **gemm** with multiple subtensors $\underline{\mathbf{A}}'_{\pi', q}$ and $\underline{\mathbf{C}}'_{\pi', q}$ with $\pi' = (\pi_1, \dots, \pi_{\hat{q}-1})$.

Both algorithm variants will be referred to as **<par-loops, seq-gemm>** which can be used with subtensors or tensor slices. Note that **<seq-loops, par-gemm>** and **<par-loops, seq-gemm>** are opposing versions where either **gemm** or the free loops are performed in parallel. The all-parallel version **<par-loops, par-gemm>** executes available loops in parallel where each loop thread executes a multi-threaded **gemm** with either subtensors or tensor slices.

Multithreaded batched Matrix Multiplication The next version of the base algorithm is a modified version of the general subtensor-matrix approach that calls a single batched **gemm** for the eighth case. The subtensor dimensions and remaining **gemm** arguments remain the same. The library implementation is responsible how subtensor-matrix multiplications are executed and if subtensors are further divided into smaller subtensors or tensor slices. This version will be referred to as the **<gemm_batch>** variant.

5 Experimental Setup

Computing System The experiments have been carried out on an Intel Xeon Gold 6248R processor with a Cascade micro-architecture. The processor consists of 24 cores operating at a base frequency of 3 GHz for non-AVX512 instructions. With 24 cores and a peak AVX-512 boost frequency of 2.5 GHz, the processor achieves a theoretical data throughput of ca. 1.92 double precision Tflops. We measured a peak performance of 1.78 double precision Tflops using the likwid performance tool.

The source code has been compiled with GCC v10.2 using the highest optimization level -O3 and -march=native, -pthread and -fopenmp. Loops within for the eighth case have been parallelized using GCC's OpenMP v4.5 implementation. We have used the **gemv** and **gemm** implementation of the 2024.0 Intel MKL and its own threading library **mk1_intel_thread** together with the threading runtime library **libiomp5**.

If not otherwise mentioned, both tensors $\underline{\mathbf{A}}$ and $\underline{\mathbf{C}}$ are stored according to the first-order linear tensor layout with $\pi = (1, \dots, p)$ whereas matrix \mathbf{B} has the row-major storage format.

Tensor Shapes We have used asymmetrically-shaped and symmetrically-shaped tensors in order to cover many possible use cases. The dimension tuples of both shape types are organized within two three-dimensional arrays with which tensors are initialized. The dimension array for the first shape type contains $720 = 9 \times 8 \times 10$ dimension tuples where the row number is the tensor order ranging from 2 to 10. For each tensor order 8 tensor instances with increasing tensor size is generated. The second set consists of $336 = 6 \times 8 \times 7$ dimensions

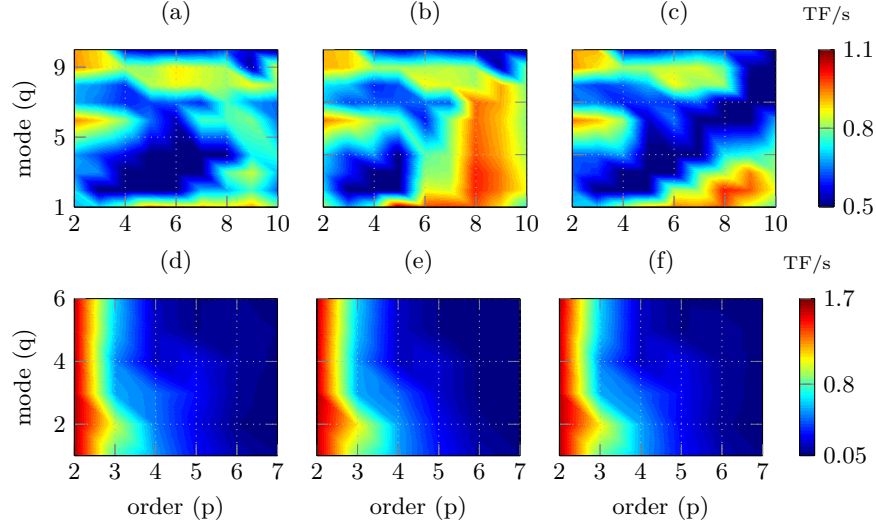


Fig. 1. Performance maps in double-precision Tflops of the proposed algorithms with varying tensor orders p and contraction modes q . Tensors are asymmetrically-shaped on the upper plots and symmetrically-shaped on the lower plots. In (a) and (d) function `<gemm_batch>` is executed, in (b) and (e) `<par-loops,seq-gemm>` with tensor slices, in (c) and (f) `<par-loops,seq-gemm>` with subtensors.

339 tuples where the tensor order ranges from 2 to 7 and has 8 dimension tuples for
 340 each order. Each tensor dimension within the second set is 2^{12} , 2^8 , 2^6 , 2^5 , 2^4 and
 341 2^3 . A detailed explanation of the tensor shape setup is given in [2,3].

342 6 Results and Discussion

343 **Slicing Methods** The following paragraphs analyze the two proposed slicing
 344 methods by benchmarking the functions `<par-loops,seq-gemm>` and `<gemm_batch>`
 345 using asymmetrically (top) and symmetrically (bottom) shaped tensors. Fig. 1
 346 contains six contour plots (performance maps) in which `<par-loops,seq-gemm>`
 347 either uses subtensors or tensor slices and `<gemm_batch>` loops over subtensors
 348 only. Each point within the performance map represents a mean value that has
 349 been averaged over tensor sizes for a tensor order¹.

350 For asymmetrically shaped tensors, function `<par-loops,seq-gemm>` with ten-
 351 sor slices performs on average 18% better than with subtensors. Our function
 352 `<par-loops,seq-gemm>` with tensor slices is on average 11% faster than Intel’s
 353 `gemm_batch` routine and reaches almost 1.1 Tflops for non-edge cases with $q > 2$
 354 and $p > 6$. This suggests that the Intel’s implementation does not divide sub-
 355 tensors into smaller blocks.

¹ Note that Fig. 2 suggests that the contraction mode q can be greater than p which is not possible. Our profiling program sets $q = p$ in such cases.

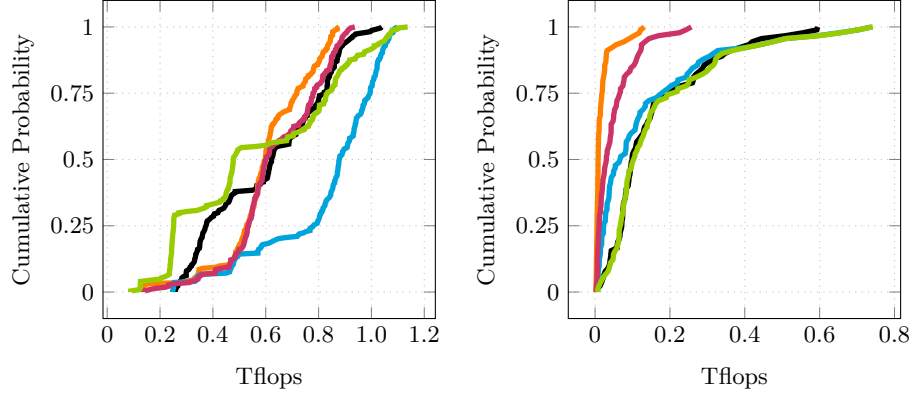


Fig. 2. Cumulative performance distributions of the proposed algorithms for the eighth case. Each distribution line belongs to one algorithm: `<gemm_batch>` (black), `<seq-loops,par-gemm>` (orange) and `<par-loops,seq-gemm>` (blue) using tensor slices, `<seq-loops,par-gemm>` (pink) and `<par-loops,seq-gemm>` (green) using subtenors. Tensors are asymmetrically (left plot) and symmetrically shaped (right plot).

356 With symmetrically shaped tensors, `<par-loops,seq-gemm>` with tensor slices
 357 performs almost identical as `<gemm_batch>` with 221.52 Gflops and 236.21 Gflops,
 358 respectively. Moreover, the slicing method seems to have only little affect on the
 359 overall runtime behavior of `<par-loops,seq-gemm>`. In contrast to the perfor-
 360 mance maps with asymmetrically shaped tensors, all functions almost reach the
 361 attainable peak performance of 1.7 Tflops when $p = 2$. This can be by the fact that
 362 both dimensions are equal or larger than 4096 enabling `gemm` to operate under
 363 optimal conditions.

364 **Parallelization Methods** The contour plots in Fig. 1 contain performance
 365 data of all cases except for 4 and 5, see Table 1. The effects of the presented slic-
 366 ing and parallelization methods can be better understood if performance data of
 367 only the eighth case is examined. Fig. 2 contains cumulative performance distri-
 368 butions of all the proposed algorithms which are generated `gemm` or `gemm_batch`
 369 calls within case 8. As the distribution is empirically generated, the probability
 370 y of a point (x, y) on a distribution function corresponds to the number of test
 371 cases of a particular algorithm that achieves x or less Tflops. For instance, func-
 372 tion `<seq-loops,par-gemm>` with subtenors computes the tensor-matrix product
 373 with equal to or less than 0.6 Tflops for 50% percent of the test cases using
 374 asymmetrically shaped tensor. Consequently, distribution functions with an ex-
 375 ponential growth is favorable while logarithmic behavior is less desirable. The
 376 test set cardinality for case 8 is 255 for asymmetrically shaped tensors and 91
 377 for symmetrically ones.

378 In case of asymmetrically shaped tensors, `<par-loops,seq-gemm>` with tensor
 379 slices performs best and outperforms `<gemm_batch>`. One unexpected finding is
 380 that function `<seq-loops,par-gemm>` with any slicing strategy performs better

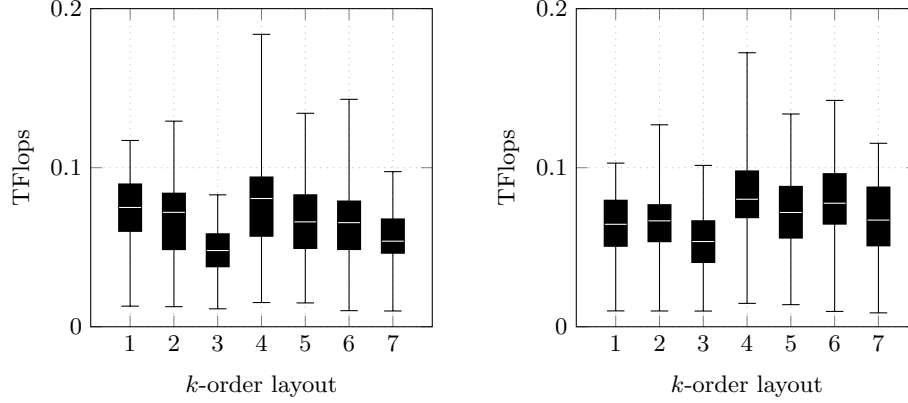


Fig. 3. Box plots visualizing performance statics in double-precision Tflops of `<gemm_batch>` (left) and `<par-loops, seq-gemm>` with subtensors (right). Box plot number k denotes the k -order tensor layout of symmetrically shaped tensors with order 7.

than `<gemm_batch>` when the tensor order p and contraction mode q satisfy $4 \leq p \leq 7$ and $2 \leq q \leq 4$, respectively. Functions executed with symmetrically shaped tensors reach at most 743 Gflops for the eighth case which is less than half of the attainable peak performance of 1.7 Tflops. This is expected as cases 2 and 3 are not considered. Functions `<par-loops, seq-gemm>` with subtensors and `<gemm_batch>` have almost the same performance distribution outperforming `<seq-loops, par-gemm>` for almost every test case. Function `<par-loops, seq-gemm>` with tensor slices is on average almost as fast as with subtensors. However, if the tensor order is greater than 3 and the tensor dimensions are less than 64, its running time increases by almost a factor of 2.

These observations suggest to use `<par-loops, seq-gemm>` with tensor slices for common cases in which the leading and contraction dimensions are larger than 64 elements. Subtensors should only be used if the leading dimension n_{π_1} of $\underline{\mathbf{A}}_{\pi_1, q}$ and $\underline{\mathbf{C}}_{\pi_1, q}$ falls below 64. This strategy is different to the one presented in [8] that maximizes the number of modes involved in the matrix multiply. We have also observed no performance improvement if `par-gemm` was used with `par-loops` which is why their distribution functions are not shown in Fig. 2. Moreover, in most cases the `seq-loops` implementations are independent of the tensor shape slower than `par-loops`, even for smaller tensor slices.

Layout-Oblivious Algorithms Fig. 3 contains two subfigures visualizing performance statics in double-precision Tflops of `<gemm_batch>` (left subfigure) and `<par-loops, seq-gemm>` with subtensors (right subfigure). Each box plot with the number k has been computed from benchmark data with symmetrically shaped order-7 tensors with the k -order tensor layout. The 1-order and 7-order layout are the first- and last-order storage formats for the order-7 tensor with $\pi_F = (1, 2, \dots, 7)$ and $\pi_L = (7, 6, \dots, 1)$. The definition of k -order tensor layouts can be found in section 3.

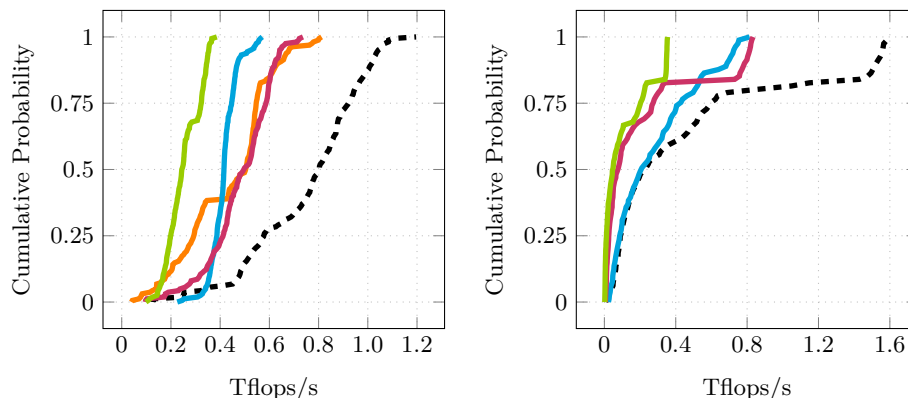


Fig. 4. Cumulative performance distributions of tensor-times-matrix algorithms in double-precision Tflops. Each distribution line belongs to a library: **tlib**[ours] (---), **tcl** (—), **tblis** (—), **libtorch** (—), **eigen** (—). Libraries have been tested with asymmetrically-shaped (left plot) and symmetrically-shaped tensors (right plot).

408 The low performance of around 70 Gflops can be attributed to the fact that
 409 the contraction dimension of subtensors of tensor slices of symmetrically shaped
 410 order-7 tensors are 8 while the leading dimension is 8 or at most 48 for subtensors.
 411 The relative standard deviation of `<gemm_batch>`'s and `<par-loops,seq-gemm>`'s
 412 median values are 12.95% and 17.61%. Their respective interquartile range are
 413 similar with a relative standard deviation of 22.25% and 15.23%.

414 The runtime results with different k -order tensor layouts show that the per-
 415 formance of our proposed algorithms is not designed for a specific tensor layout.
 416 Moreover, the performance stays within an acceptable range independent of the
 417 tensor layout.

418 **Comparison with other Approaches** We have compared our best imple-
 419 mentation with four libraries that implement the tensor-matrix multiplication
 420 using different approaches. Library **tcl** implements the TTGT approach with
 421 a high-perform tensor-transpose library **hptt** which is discussed in [15]. **tblis**
 422 implements the GETT approach that is akin to Blis' algorithm design for the
 423 matrix multiplication [10]. The tensor extension of **eigen** (v3.3.7) is used by the
 424 Tensorflow framework. Library **libtorch** (v2.3.0) is the C++ distribution of Py-
 425 Torch. **tlib** denotes our library using algorithm `<par-loops,seq-gemm>` that have
 426 been presented in the previous paragraphs.

427 Fig. 2 contains cumulative performance distributions for the complete test
 428 sets comparing the performance distribution of our implementation with the pre-
 429 viously mentioned libraries. Note that we only have used tensor slices for asym-
 430 metrically shaped tensors (left plot) and subtensors for symmetrically shaped
 431 tensors (right plot). Our implementation with a median performance of 793.75
 432 Gflops outperforms others' for almost every asymmetrically shaped tensor in the
 433 test set. The median performances of **tcl**, **tblis**, **libtorch** and **eigen** are 503.61,

434 415.33, 496.22 and 244.69 Gflops reaching on average 74.11%, 61.14%, 76.68%
 435 and 39.34% of **tlib**'s throughputs.

436 In case of symmetrically shaped tensors the performance distributions of all
 437 libraries on the right plot in Fig. 2 are much closer. The median performances of
 438 **tlib**, **tblis**, **libtorch** and **eigen** are 228.93, 208.69, 76.46, 46.25 Gflops reaching
 439 on average 73.06%, 38.89%, 19.79% of **tlib**'s throughputs². All libraries operate
 440 with 801.68 or less Gflops for the cases 2 and 3 which is almost half of **tlib**'s
 441 performance with 1579 Gflops. The median performance and the interquartile
 442 range of **tblis** and **tlib** for the cases 6 and 7 are almost the same. Their respective
 443 median Gflops are 255.23 and 263.94 for the sixth case and 121.17 and 144.27
 444 for the seventh case. This explains the similar performance distributions when
 445 their performance is less than 400 Gflops. **Libtorch** and **eigen** compute the
 446 tensor-matrix product, in median, with 17.11 and 9.64 Gflops/s, respectively.
 447 Our library **tlib** has a median performance of 102.11 Gflops and outperforms
 448 **tblis** with 79.35 Gflops for the eighth case.

449 7 Conclusion and Future Work

450 We presented efficient layout-oblivious algorithms for the compute-bound tensor-
 451 matrix multiplication which is essential for many tensor methods. Our approach
 452 is based on the LOG-method and computes the tensor-matrix product in-place
 453 without transposing tensors. It applies the flexible approach described in [2] and
 454 generalizes the findings on tensor slicing in [8]. The resulting algorithms are able
 455 to process dense tensors with arbitrary tensor order, dimensions and with any
 456 linear tensor layout all of which can be runtime variable.

457 Our benchmarks show that dividing the base algorithm into eight different
 458 **gemm** cases improves the overall performance. We have demonstrated that algo-
 459 rithms with parallel loops over single-threaded **gemm** calls with tensor slices and
 460 subtensors perform best. Interestingly, they outperform a single **gemm_batch** call
 461 with subtensors, on average, by 14% in case of asymmetrically shaped tensors
 462 and if tensor slices are used. Both version computes the tensor-matrix product on
 463 average faster than other state-of-the-art implementations. We have shown that
 464 our algorithms are layout-oblivious and do not need further refinement if the ten-
 465 sor layout is changed. We measured a relative standard deviation of 12.95% and
 466 17.61% with symmetrically-shaped tensors for different k -order tensor layouts.

467 Summarizing our findings, LOG-based tensor-times-matrix algorithms are
 468 able to outperform TTGT-based and GETT-based implementations without
 469 losing their flexibility. Hence, other actively developed libraries such as LibTorch
 470 and Eigen will benefit from implementing the proposed algorithms. Our header-
 471 only library provides C++ interfaces and a python module which allows frame-
 472 works to easily integrate our library.

473 In the future, we intend to generalize LOG-based approach for general ten-
 474 sor contractions with the same flexibility that we offered for the tensor-matrix

² We were unable to run tcl with our test set containing symmetrically shaped tensors.
 We suspect a very high memory demand to be the reason.

475 multiplication. We would like to further optimize the tensor-matrix multiplica-
 476 tion based on benchmark results of matrix-matrix products which might lead to
 477 better runtime results for edge cases.

478 **Source Code Availability** Project description and source code can be found
 479 at <https://github.com/bassoy/ttm>. The sequential tensor-matrix multiplication of
 480 TLIB is part of uBLAS and in the official release of **Boost v1.70.0** and later.

481 References

- 482 1. Bader, B.W., Kolda, T.G.: Algorithm 862: Matlab tensor classes for fast algorithm
 483 prototyping. *ACM Trans. Math. Softw.* **32**, 635–653 (December 2006)
- 484 2. Bassoy, C.: Design of a high-performance tensor-vector multiplication with blas.
 485 In: *International Conference on Computational Science*. pp. 32–45. Springer (2019)
- 486 3. Bassoy, C., Schatz, V.: Fast higher-order functions for tensor calculus with tensors
 487 and subtensors. In: *International Conference on Computational Science*. pp. 639–
 488 652. Springer (2018)
- 489 4. Goto, K., Geijn, R.A.v.d.: Anatomy of high-performance matrix multiplication.
 490 *ACM Transactions on Mathematical Software (TOMS)* **34**(3) (2008)
- 491 5. Karahan, E., Rojas-López, P.A., Bringas-Vega, M.L., Valdés-Hernández, P.A.,
 492 Valdes-Sosa, P.A.: Tensor analysis and fusion of multimodal brain images. *Pro-
 493 ceedings of the IEEE* **103**(9), 1531–1559 (2015)
- 494 6. Kolda, T.G., Bader, B.W.: Tensor decompositions and applications. *SIAM review*
 495 **51**(3), 455–500 (2009)
- 496 7. Lee, N., Cichocki, A.: Fundamental tensor operations for large-scale data analysis
 497 using tensor network formats. *Multidimensional Systems and Signal Processing*
 498 **29**(3), 921–960 (2018)
- 499 8. Li, J., Battaglino, C., Perros, I., Sun, J., Vuduc, R.: An input-adaptive and in-place
 500 approach to dense tensor-times-matrix multiply. In: *High Performance Computing,
 501 Networking, Storage and Analysis*, 2015. pp. 1–12. IEEE (2015)
- 502 9. Lim, L.H.: Tensors and hypermatrices. In: Hogben, L. (ed.) *Handbook of Linear
 503 Algebra*. Chapman and Hall, 2 edn. (2017)
- 504 10. Matthews, D.A.: High-performance tensor contraction without transposition.
 505 *SIAM Journal on Scientific Computing* **40**(1), C1–C24 (2018)
- 506 11. Napoli, E.D., Fabregat-Traver, D., Quintana-Ortí, G., Bientinesi, P.: Towards an
 507 efficient use of the blas library for multilinear tensor contractions. *Applied Math-
 508 ematics and Computation* **235**, 454 – 468 (2014)
- 509 12. Papalexakis, E.E., Faloutsos, C., Sidiropoulos, N.D.: Tensors for data mining and
 510 data fusion: Models, applications, and scalable algorithms. *ACM Transactions on
 511 Intelligent Systems and Technology (TIST)* **8**(2), 16 (2017)
- 512 13. Shi, Y., Niranjan, U.N., Anandkumar, A., Cecka, C.: Tensor contractions with
 513 extended blas kernels on cpu and gpu. In: *2016 IEEE 23rd International Conference
 514 on High Performance Computing (HiPC)*. pp. 193–202 (Dec 2016)
- 515 14. Solomonik, E., Matthews, D., Hammond, J., Demmel, J.: Cyclops tensor frame-
 516 work: Reducing communication and eliminating load imbalance in massively par-
 517 allel contractions. In: *Parallel & Distributed Processing (IPDPS)*, 2013 IEEE 27th
 518 International Symposium on. pp. 813–824. IEEE (2013)

- 519 15. Springer, P., Bientinesi, P.: Design of a high-performance gemm-like tensor–tensor
520 multiplication. *ACM Transactions on Mathematical Software (TOMS)* **44**(3), 28
521 (2018)